



ELSEVIER

Finite Elements in Analysis and Design 38 (2002) 999–1012

FINITE ELEMENTS
IN ANALYSIS
AND DESIGN

www.elsevier.com/locate/finel

Characteristics of semi- and full discretization of stabilized Galerkin meshfree method

Yang You^a, Jiun-Shyan Chen^{a,*}, Thomas E. Voth^{b,1}

^a*Department of Civil & Environmental Engineering, University of California, Los Angeles, 5731G Boelter Hall, Los Angeles, CA, 90095-1593, USA*

^b*Thermal Science Department, Sandia National Laboratories, M/S 0819, P.O. Box 5800, Albuquerque, NM, 87185-0819, USA*

Abstract

Stabilized conforming nodal integration (SCNI) has been developed to enhance computational efficiency of Galerkin meshfree methods. This paper employs von Neumann analyses to study the spatial semi-discretization of Galerkin meshfree methods using SCNI. Two model problems were presented with respect to the normalized phase speed and group speed for the wave equation, and normalized diffusivity for the heat equation. Both consistent and lumped mass (capacity) discretizations are considered in the study. The transient properties in the full discretization of the two model problems were also analyzed. The results show superior dispersion behavior in meshfree methods integrated by SCNI compared to the Gauss integration when consistent mass (capacity) matrix is employed in the discretization. For the lumped mass case, SCNI performance is comparable to that of the Gauss integration, but exhibits considerable reduction of computational time. © 2002 Elsevier Science B.V. All rights reserved.

Keywords: Stabilized conforming nodal integration; Meshfree methods; Reproducing kernel particle method; Discretization error

1. Introduction

Conventional Galerkin meshfree methods employ Gauss quadrature in the integration of the weak form [1–5]. The intrinsic feature of the meshfree approximation theory, however, is not consistent with this integration technique. Studies have shown that Gauss integration leads to considerable numerical complexity in Galerkin meshfree method. Higher-order Gauss quadrature rules are required

* Corresponding author.

E-mail address: jschen@seas.ucla.edu (J.-S. Chen).

¹ Sandia is a multi-program laboratory operated by Sandia Corporation for the United States Department of Energy under Contract DE-AC04-94AL85000.

to minimize the error due to mismatching between shape function supports and the integration cells [6]. In addition, Gauss integration does not satisfy linear exactness in the Galerkin approximation with arbitrary discretization [7]. A stabilized conforming nodal integration (SCNI) [7] has been developed to address the integration issue in meshfree methods with enhanced efficiency and accuracy. In this approach, a strain smoothing stabilization has been proposed to provide a stabilization of nodal integration. The gradient matrix associated with the strain smoothing stabilization also satisfies integration constraints and therefore meets linear exactness in the Galerkin method. Studies have shown that SCNI significantly reduces computational effort with almost no loss of accuracy in boundary value problems. In fact, since Gauss integration violates integration constraints, SCNI provides better solution accuracy in meshfree methods than that of Gauss integration, particularly when discrete nodal spacing is nonuniform [7].

The aforementioned studies were limited to static boundary value problems. This paper focuses on the assessment of the numerical performance of SCNI meshfree methods in transient problems. The investigation of the dispersive errors associated with discrete solutions has been used by numerous researchers to characterize the numerical performance of certain discretization methods. The dispersion characteristic of reproducing kernel particle method (RKPM) semi-discretization with traditional Gauss integration and direct nodal integration has been studied by Voth and Christon [8]. It has been shown that, with the consistent mass, fully Gauss-integrated RKPM formulation yields the best numerical dispersion behavior. For the second-order wave equation, the aforementioned approach requires only three to four particles per wavelength for a phase error less than 5%. Finite element, on the other hand, requires ten nodes to reach the same level of accuracy in phase speed. In addition, it has been noted that the application of direct nodal integration introduces substantial degradation in the behavior of the phase speed and diffusivity.

This paper employs von Neumann analysis to investigate SCNI effects on the characteristics of meshfree semi-discretization in space. The combined effects of spatial and temporal discretizations are also investigated with respect to transient analysis. Section 2 reviews integration constraints and SCNI for Galerkin meshfree methods. Section 3 presents the formulation of the von Neumann analysis for parabolic and hyperbolic model problems. The results of dispersion analysis for meshfree methods using direct nodal integration, SCNI, and Gauss integration are presented. The characteristics of meshfree full discretization in transient analysis are discussed in Section 4. Final conclusions are drawn in Section 5.

2. Meshfree approximation and stabilized conforming nodal integration

2.1. Meshfree approximation

The first generation of meshfree methods, the smoothed particle dynamics (SPH) [9], introduced kernel approximation and collocation of the conservation laws to formulate a system of discrete equations. More recent meshfree methods, such as the element free Galerkin (EFG) [1], partition of unity method (PUM) [2], reproducing kernel particle method [4], and HP-Cloud [3], are collectively referred to as Galerkin meshfree methods. Galerkin meshfree methods are distinct from SPH in two ways: (1) consistency is introduced to correct kernel estimates, and (2) discretization is based on a weak form and Galerkin approximation, rather than direct collocation. With

respect to the first distinction, consistency is imposed in the construction of shape function $\Psi_I(\mathbf{x})$, resulting in:

$$\Psi_I(\mathbf{x}) = C(\mathbf{x}; \mathbf{x} - \mathbf{x}_I)\Phi_a(\mathbf{x} - \mathbf{x}_I), \tag{1}$$

where $\Phi_a(\mathbf{x} - \mathbf{x}_I)$ is the kernel function used in the kernel estimate and $C(\mathbf{x}; \mathbf{x} - \mathbf{x}_I)$ is the correction function obtained either from moving least squares (MLS) or the reproducing kernel (RK) approximation:

$$C(\mathbf{x}; \mathbf{x} - \mathbf{x}_I) = \mathbf{H}^T(\mathbf{0})\mathbf{M}^{-1}(\mathbf{x})\mathbf{H}(\mathbf{x} - \mathbf{x}_I), \tag{2}$$

where $\mathbf{H}^T(\mathbf{x} - \mathbf{x}_I) = \{1, x_1 - x_{1I}, x_2 - x_{2I}, \dots, (x_3 - x_{3I})^n\}$ is the vector of monomial basis functions, and $\mathbf{M}(\mathbf{x})$ is the Gram matrix of monomial basis functions with respect to kernel $\Phi_a(\mathbf{x} - \mathbf{x}_I)$. These set of shape functions $\Psi_I(\mathbf{x})$ satisfy

$$\sum_{I=1}^{NP} \Psi_I(\mathbf{x})x_{1I}^i x_{2I}^j x_{3I}^k = x_1^i x_2^j x_3^k; \quad 0 \leq i + j + k \leq n. \tag{3}$$

2.2. Stabilized conforming nodal integration

Conventionally, the discrete equations of Galerkin meshfree methods are formulated by introducing shape functions, Eqs. (1)–(2), in the approximation of unknown variables and employing the Gauss quadrature rule for the integration of weak form. For Gauss integration to be accurate, the integrated function cannot terminate in the interior of the integration cells [6]. Unfortunately, this constraint is difficult to meet, particularly for a nonuniform node distribution. Errors induced by the inconsistent arrangement between the shape function supports and the integration cell can be minimized using very fine integration cells with high-order quadrature rules. These procedures are, however, computationally quite costly. Another drawback in Gauss integration for meshfree methods is that it does not meet linear exactness in the Galerkin approximation even if the shape functions have linear consistency [6,7]. The requirements to obtain an exact solution of a second order value problem when the solution is linear (linear exactness) are: (1) shape functions are linearly consistent, and (2) integration of the weak form meets integration constraints. The first requirement can be easily satisfied by employing linear basis functions in \mathbf{H} of Eq. (2). The second condition requires that the integration of the weak form meet the following integration constraint:

$$\sum_{L=1}^{NIT} \nabla \Psi_I(\mathbf{x}_L)\omega_L = \mathbf{0} \quad \text{for } \{I : \text{supp}(\Psi_I) \cap \Gamma = \emptyset\}, \tag{4}$$

where Γ is the total boundary, \mathbf{x}_L is the integration points, ω_L is the weight, and NIT is the number of integration points. For shape functions that intersect essential boundaries, a similar condition can be obtained by enforcing flux equilibrium [7].

A stabilized conforming nodal integration [7] was proposed to improve efficiency and correct some drawbacks in Galerkin meshfree methods. The SCNI method is based on an assumed strain method, in which a modified gradient is introduced at the integration point (nodal point) in order to meet

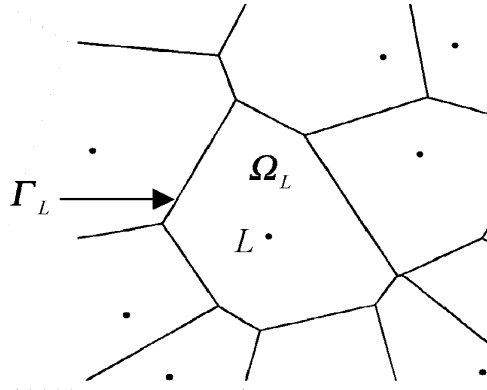


Fig. 1. Two-dimensional Voronoi diagram.

the integration constraint in Eq. (4):

$$\tilde{\nabla} u_i^h(\mathbf{x}_L) = \frac{1}{A_L} \int_{\Omega_L} \nabla u_i^h \, d\Omega = \frac{1}{A_L} \int_{\Gamma_L} \mathbf{n} u_i^h \, d\Gamma = \sum_I \tilde{\nabla} \Psi_I(x_L) d_{iI}, \tag{5}$$

$$\tilde{\nabla} \Psi_I(\mathbf{x}_L) = \frac{1}{A_L} \int_{\Gamma_L} \Psi_I(\mathbf{x}) \mathbf{n}(\mathbf{x}) \, d\Gamma, \tag{6}$$

where Ω_L and Γ_L are the representative domain and boundary, respectively, of node L obtained from, for example, the Voronoi diagram in Fig. 1, and A_L is the area (or volume) of Ω_L . It can be easily shown that the smoothed gradient $\tilde{\nabla} \Psi_I(\mathbf{x})$ meets the integration constraint in Eq. (4). By employing the assumed strain method with the smoothed strain in Eq. (6), and introducing nodal integration to the weak form, the final stiffness matrix for the elasticity problem is

$$\mathbf{K}_{IJ} = \sum_{L=1}^{NP} \tilde{\mathbf{B}}_I^T(\mathbf{x}_L) \mathbf{D} \tilde{\mathbf{B}}_J(\mathbf{x}_L) A_L, \tag{7}$$

where $\tilde{\mathbf{B}}_I$ is the gradient matrix associated with the strain in elasticity constructed using Eq. (6), and \mathbf{D} is the elasticity matrix. For heat conduction, the conductivity matrix can be obtained by replacing $\tilde{\mathbf{B}}_I$ with $\tilde{\nabla} \Psi_I$ in Eq. (7).

3. von Neumann dispersion analysis

Numerical schemes tend to bring in dispersion errors to the solution. This numerical dispersion error is often used to measure the performance of the numerical method. Von Neumann dispersion analysis provides an approach to analyze this numerical dispersion error for semi-discretization in the spatial domain of the model partial differential equation.

The model problems in this study are the second-order wave equation (hyperbolic) and the heat equation (parabolic).

3.1. Second-order wave equation

The first model problem to be studied is a second-order wave equation:

$$\frac{\partial^2 u}{\partial t^2} = c^2 \left(\frac{\partial^2 u}{\partial x^2} + \frac{\partial^2 u}{\partial y^2} \right), \tag{8}$$

where c is the physical wave speed. By introducing the approximation

$$u_i(\mathbf{x}) \approx u_i^h(\mathbf{x}) = \sum_I \Psi_I(\mathbf{x}) d_{iI}, \tag{9}$$

the semi-discretization of weak form associated with Eq. (8) for infinite domain is

$$\mathbf{M}\ddot{\mathbf{d}} + \mathbf{K}\mathbf{d} = 0, \tag{10}$$

where \mathbf{K} and \mathbf{M} are the stiffness and mass matrix, respectively. Von Neumann analysis employs the discrete solution of the form

$$d(x_m, y_n) = d_0 \exp(ik(x_m \cos \theta + y_n \sin \theta) - i\bar{\omega}t), \tag{11}$$

where (x_m, y_n) is the location of discrete points, $\bar{\omega}$ is the numerical circular frequency, and k is the wave number. By considering a uniform space discretization $x_{m+i} = x_m + i\Delta x$, $y_{n+j} = y_n + j\Delta y$, and substituting Eq. (11) into Eq. (10), one obtains:

$$\begin{aligned} & -\bar{\omega}^2 \sum_{i=-I}^I \sum_{j=-J}^J \{ \mathbf{M}_{(m,n)(m+i,n+j)} \exp(ik(i\Delta x \cos \theta + j\Delta y \sin \theta)) \} \\ & + \sum_{i=-I}^I \sum_{j=-J}^J \{ \mathbf{K}_{(m,n)(m+i,n+j)} \exp(ik(i\Delta x \cos \theta + j\Delta y \sin \theta)) \} = 0. \end{aligned} \tag{12}$$

The normalized phase speed is defined as $p_n = \bar{c}/c$, where $\bar{c} = \bar{\omega}/k$ is the numerical phase speed. Using $\bar{\omega}$ from Eq. (12), the normalized phase speed is obtained:

$$p_n = \frac{1}{ck} \sqrt{\frac{\sum_{i=-I}^I \sum_{j=-J}^J \{ \mathbf{K}_{(m,n)(m+i,n+j)} \exp(ik(ih_x \cos \theta + jh_y \sin \theta)) \}}{\sum_{i=-I}^I \sum_{j=-J}^J \{ \mathbf{M}_{(m,n)(m+i,n+j)} \exp(ik(ih_x \cos \theta + jh_y \sin \theta)) \}}}. \tag{13}$$

In one dimension, the normalized phase speed for semi-discretization is reduced to

$$p_n = \frac{1}{ck} \sqrt{\frac{\sum_{i=-I}^I \mathbf{K}_{m,m+i} \cos(klh_x)}{\sum_{i=-I}^I \mathbf{M}_{m,m+i} \cos(klh_x)}} \tag{14}$$

and the normalized group speed in one dimension is defined as

$$g_n = \frac{\partial \bar{\omega} / \partial k}{c}. \tag{15}$$

3.2. Heat equation

The second model problem considered is a heat equation:

$$\frac{\partial u}{\partial t} = \alpha \left(\frac{\partial^2 u}{\partial x^2} + \frac{\partial^2 u}{\partial y^2} \right), \tag{16}$$

where u is temperature variable, and α is the diffusivity. Following similar procedures used in wave equation, the normalized diffusivity is obtained as

$$d_n = \frac{1}{\alpha k^2} \frac{\sum_{i=-I}^I \sum_{j=-J}^J \{ \mathbf{K}_{(m,n)(m+i,n+j)} \exp(ik(ih_x \cos \theta + jh_y \sin \theta)) \}}{\sum_{i=-I}^I \sum_{j=-J}^J \{ \mathbf{M}_{(m,n)(m+i,n+j)} \exp(ik(ih_x \cos \theta + jh_y \sin \theta)) \}} \tag{17}$$

and the reduced form for one dimension is

$$d_n = \frac{1}{\alpha k^2} \frac{\sum_{i=-I}^I \mathbf{K}_{m,m+i} \cos(kih_x)}{\sum_{i=-I}^I \mathbf{M}_{m,m+i} \cos(kih_x)}. \tag{18}$$

3.3. von Neumann analysis for meshfree methods

The normalized phase speed of wave equation computed by meshfree method using Gauss integration (GI), stabilized conforming nodal integration (SCNI), and direct nodal integration (DNI) were compared. Different combinations of integration methods for \mathbf{K} and \mathbf{M} were evaluated, given the following conventions: (1) GI–GI: both \mathbf{K} and \mathbf{M} were integrated using GI; (2) SCNI–GI: \mathbf{K} was integrated using SCNI and \mathbf{M} was integrated using GI; (3) SCNI–DNI: \mathbf{K} was integrated using SCNI and \mathbf{M} was integrated using DNI; (4) DNI–DNI: both \mathbf{K} and \mathbf{M} were integrated using DNI. The effects of normalized support sizes $a = 1.0, 1.5, 2.0$ (the support of each particle covers 3, 4, and 5 particles) were also studied. In the following figures, the horizontal axis is the wave number, and the vertical axis represents normalized phase speed.

Comparisons for consistent and lumped mass cases for wave equation are shown in Figs. 2 and 3, respectively. As is evident, SCNI for stiffness and GI for mass matrix provide the

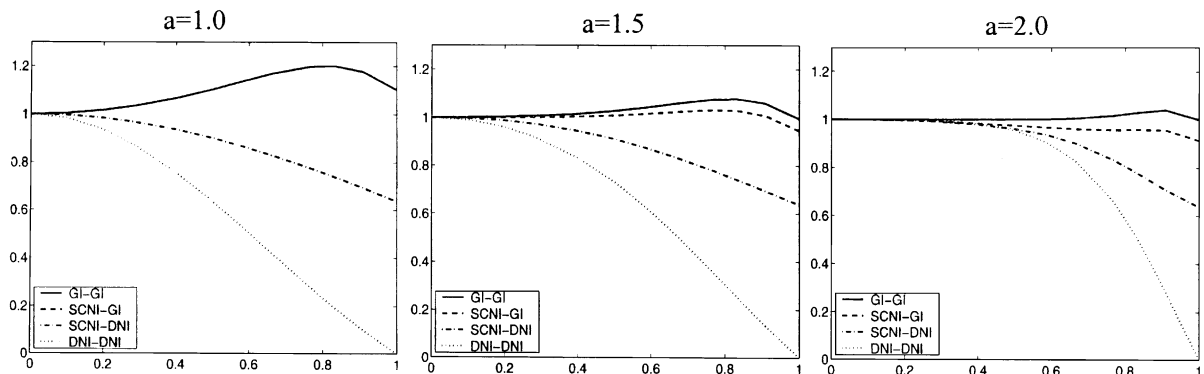


Fig. 2. Comparison of normalized phase speed using consistent mass in wave equation.

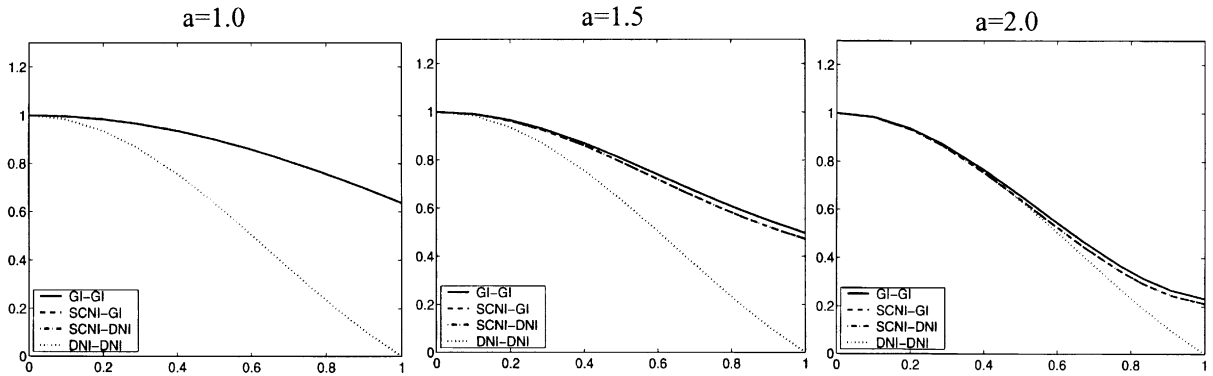


Fig. 3. Comparison of normalized phase speed using lumped mass in wave equation.

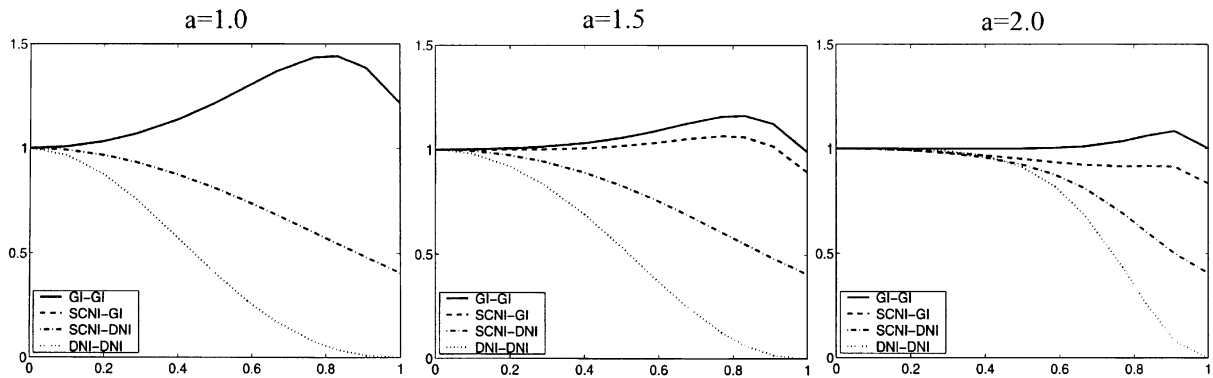


Fig. 4. Comparison of normalized diffusivity using consistent capacity in heat equation.

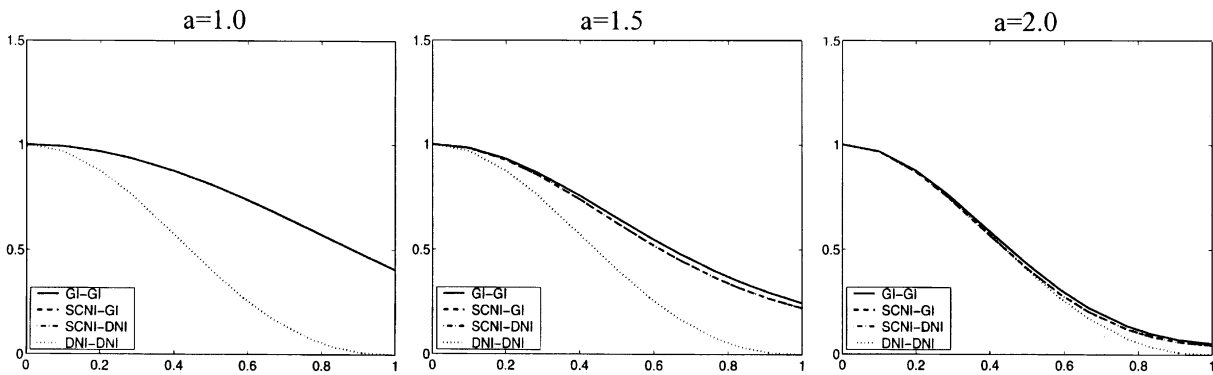


Fig. 5. Comparison of normalized diffusivity using lumped capacity in heat equation.

best performance in the consistent mass case. For lumped mass, this integration approach is comparable to that of GI–GI. It is also observed that increasing the support size yields a smaller phase error for consistent mass. For the lumped mass case, a smaller support provides the better solution. Similar behavior is observed in solution of the heat equation, for which the consistent and lumped capacity cases are shown in Figs. 4 and 5. It should also be noted that for the case where $a = 1.0$,

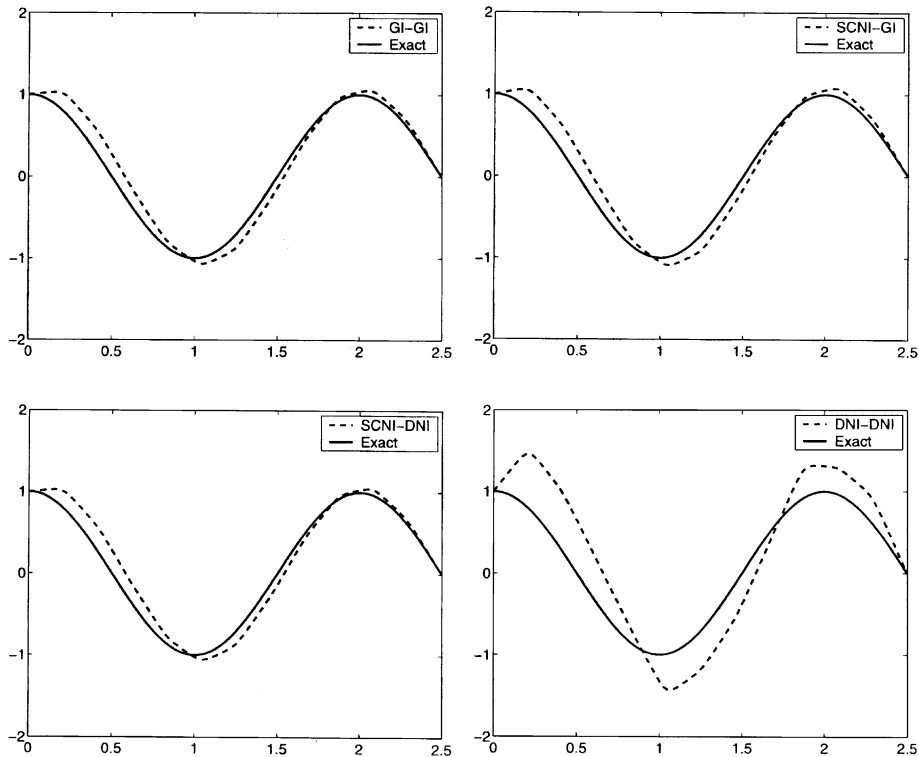


Fig. 6. Solution to Helmholtz equations with lumped mass.

the SCNI–GI and GI–GI solutions are identical. When the discretization is close to the Nyquist limit, the DNI–DNI yields stationary wave, that is, the wave does not propagate at all. This behavior is not observed for other three cases.

3.4. Helmholtz equation

In the wave propagation problem, if the phenomenon is assumed to be steady harmonic, that is

$$\bar{u}(x, t) = u(x) \exp(i\omega t), \tag{19}$$

the spatial distribution $u(x)$ is then the solution to the Helmholtz equation:

$$\Delta u + k^2 u = 0. \tag{20}$$

Since $\bar{u}(x, t)$ is harmonic in time, it serves as a very convenient tool to study the semi-discretization of the wave equation.

In the following, a one-dimensional Helmholtz equation is considered

$$\begin{aligned} u_{,xx} + k^2 u &= 0 \quad \text{in } (0, L), \\ u(0) &= 1, \quad u(L) = 0, \end{aligned} \tag{21}$$

where $k = \omega/c$ denotes the wave number. Eq. (21) is studied to verify the dispersion characteristics discussed in Section 3.3. A uniform spatial discretization was used for each case of integration

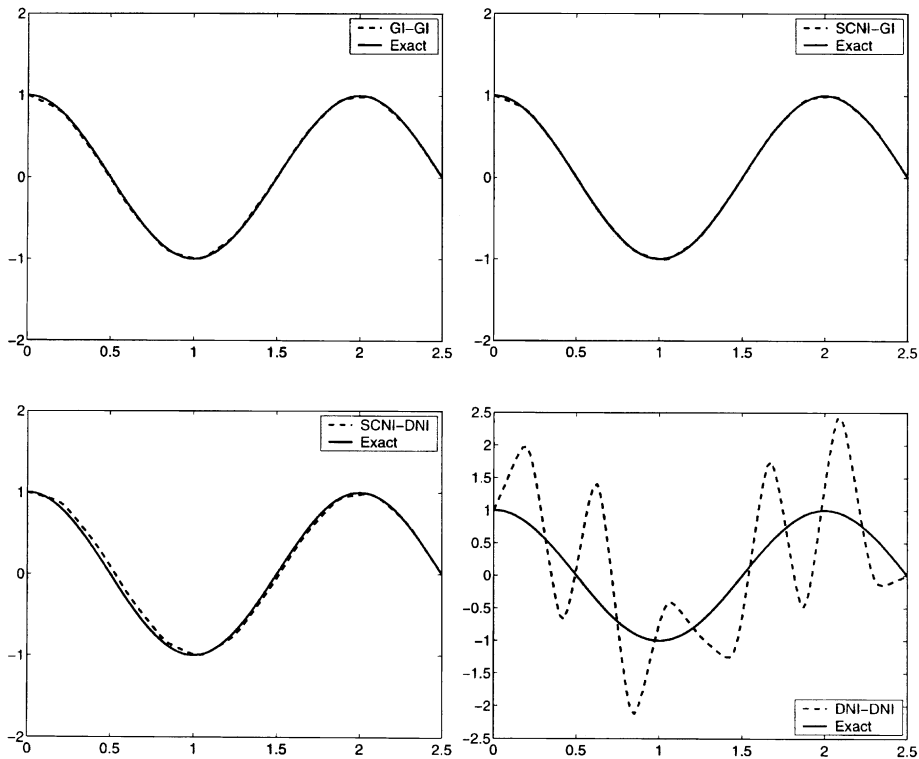


Fig. 7. Solution to Helmholtz equations with consistent mass.

procedures. Wave number $k = 3$ is used in the numerical examples, and the phase speed errors were calculated for each case. Normalized support size $a = 1.5$ is used for each particle in the construction of shape functions. The domain discretization corresponds to a nondimensional wave number $kh_x/\pi = 2h_x/\lambda = 0.2$.

The Helmholtz equation is solved using the four integration techniques with both lumped and consistent mass matrices. Fig. 6 shows the solutions of the various integration techniques with lumped mass, while those with the consistent mass were demonstrated in Fig. 7. It is observed that the behavior of the discretization errors in the numerical solution matches very well with that predicted by von Neumann dispersion analysis results in Section 3.1. SCNI–GI yields the best numerical performance among all integration methods under study. With little loss of accuracy, additional saving in computational cost can be achieved by employing SCNI–DNI in the practical implementation for both the lumped mass and the consistent mass cases.

4. Full discretization

The von Neumann analysis for the spatial semi-discretization shows that SCNI provides promising prospective in dealing with the transient problems, at least in the model problems discussed. However, it is the combined effects of space and time discretizations that are of practical importance. The

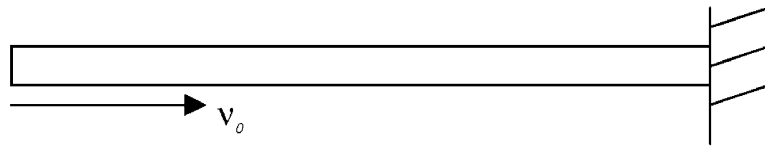


Fig. 8. Elastic bar impacting onto a rigid wall.

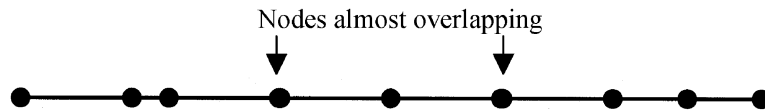


Fig. 9. Nonuniform particle distribution for lumped mass with explicit time integration.

intention of this section is not to seek the best way for the time integration procedure for the Galerkin meshfree method, but rather employ the standard explicit and implicit time integration to the transient problems, and investigate the numerical performance of the newly developed SCNI.

4.1. One-dimension wave equation

In this section, a one-dimension wave equation problem is tested. Consider an elastic bar impacting onto a rigid wall with initial velocity v_0 as shown in Fig. 8.

The governing equation for this problem is given as

$$\begin{aligned} \rho \ddot{u} &= E u_{,xx} \text{ in } (0, L), \\ u_{,x}(0, t) &= 0, \quad u(L, t) = 0, \\ u(x, 0) &= 0, \quad \dot{u}(x, 0) = v_0, \end{aligned} \quad (22)$$

where $E = 100$, $\rho = 0.01$, and $L = 10$.

The Newmark's family of time integration is used: the explicit central difference method is used with lumped mass, and the implicit average acceleration method is used with consistent mass.

In the first case, lumped mass with explicit time integration is studied. Nonuniform spatial discretization shown in Fig. 9 was used to investigate the sensitivity of discretization uniformity to the numerical solution. The wave propagation at the center node is plotted.

It is observed in Fig. 10 that the nonuniformity introduced large phase error and amplitude error in the solution by GI–GI, while the solution by DNI–DNI simply diverges. On the other hand, the two cases using SCNI are quite satisfactory. Even the case SCNI–DNI, whose result is about the same with SCNI–GI, shows small discretization error with less computational time. The time step in this problem is chosen such that the procedure GI–GI yields a convergent solution. The stability issue is not in the scope of this study, and will be studied in the future work.

In the next case, consistent mass with implicit time integration is considered. A more severe nonuniform discretization as shown in Fig. 11 is employed to identify the performance of various domain integration methods.

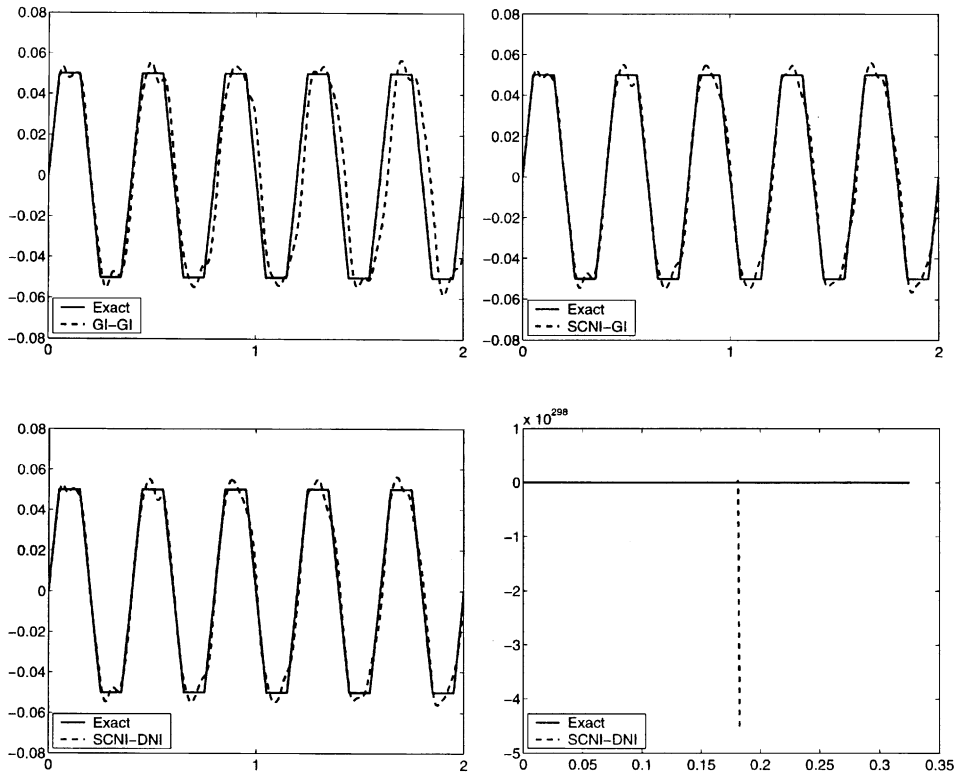


Fig. 10. Solution to wave equation with nonuniform discretization and explicit time integration.

Again, the nonuniformity in the discretization deteriorates the solution accuracy of GI-GI greatly. Although the implicit time integration guarantees convergence of the solution by DNI-DNI, it does not converge to the exact solution. SCNI-GI, as usual, shows the best accuracy among all procedures. SCNI-DNI appears to have large phase error and magnitude error, which are about the same level as GI-GI (Fig. 12).

4.2. One-dimension heat equation

The following one-dimension heat conduction equation is studied:

$$\begin{aligned} \frac{\partial U}{\partial t} &= \frac{\partial^2 U}{\partial x^2} \quad \text{in } \left(-\frac{\pi}{2}, \frac{\pi}{2}\right), \\ U(x, 0) &= U_0 + U_1 \cos(kx), \\ U(x, t) &\equiv U_0 \quad \text{on } \Gamma, \end{aligned} \tag{23}$$

where $U_0 = 1.0, U_1 = 1.0$, and $k = 3.0$ are used for initial and boundary conditions.

For this problem, the solution of uniform particle distribution with 5, 9, and 13 nodes were obtained to study the convergence behavior of each integration procedure. Both Forward Euler explicit

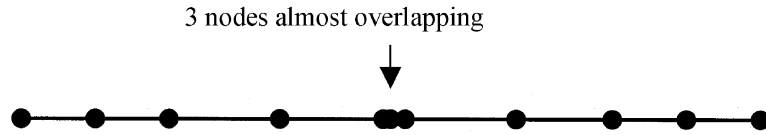


Fig. 11. Nonuniform particle distribution for consistent mass with implicit time integration.

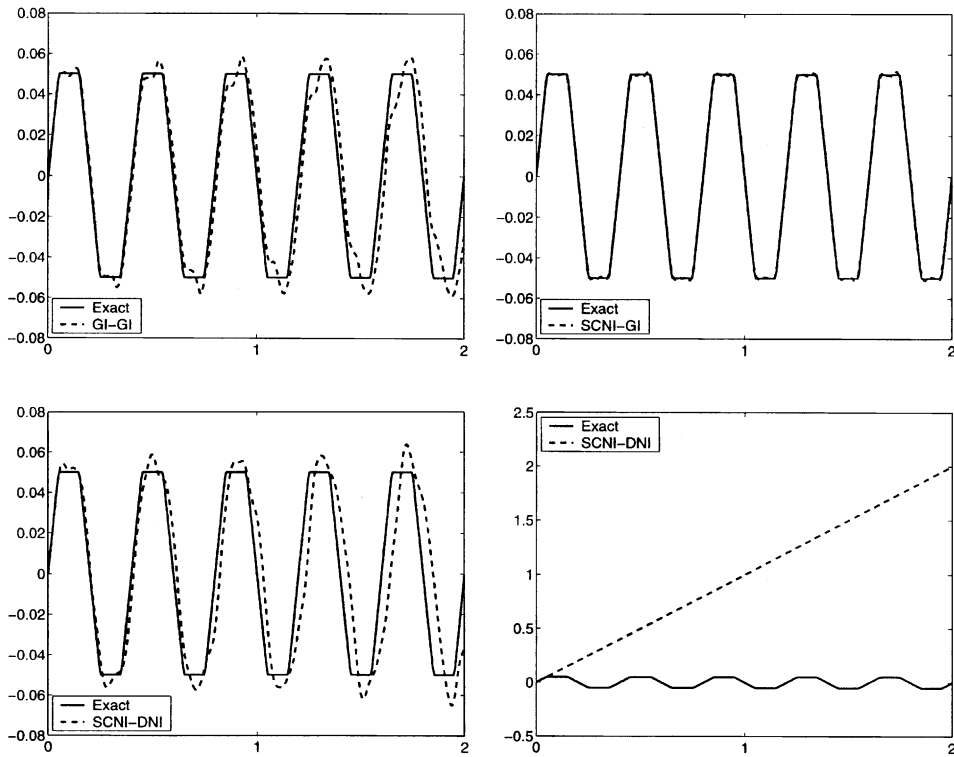


Fig. 12. Solution to wave equation with nonuniform discretization and implicit time integration.

time integration with lumped capacity, and Crank–Nicolson implicit time integration with consistent capacity were investigated.

The solution of the four domain integration methods using explicit time integration with lumped capacity matrix is shown first. The results of the temperature evolution at the center node $x = 0$ were plotted in Fig. 13. It is observed that GI–GI, SCNI–GI, and SCNI–DNI display about the same level of convergence. The error in transient analysis is in good agreement with those observed in the semi-discretization von Neumann analysis.

Similar to the semi-discretization, GI–GI and SCNI–GI show superior convergence over the other two methods, while SCNI–DNI has great improvement in accuracy over the case of DNI–DNI while maintaining low cost compared to GI–GI and SCNI–GI. A similar trend is observed in the case of implicit time integration with consistent mass as shown in Fig. 14.

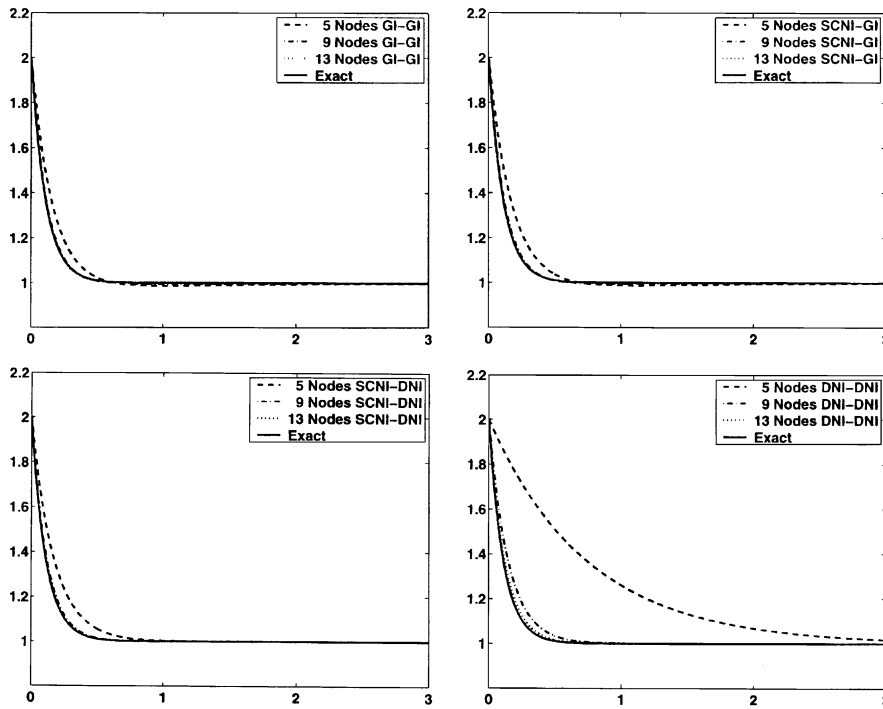


Fig. 13. Solution to heat equation with lumped capacity matrix.

5. Conclusion

Through the von Neumann analysis, the discretization characteristics of Galerkin meshfree method using the stabilized conforming nodal integration, Gauss integration, and direct nodal integration have been studied. Dispersion errors were minimized when the stiffness matrix was integrated using SCNI and consistent mass was integrated using GI. In matching SCNI for the stiffness matrix, GI performed better than DNI in the integration of the mass matrix. However, GI for the mass matrix is not of concern with respect to computational efficiency, since the mass matrix is formed only once in Lagrangian formulation. The von Neumann analysis results also show that, in the lumped mass case, dispersion errors were about the same when stiffness matrix was integrated using either SCNI or GI. It should be noted, however, that GI is computationally much more costly than SCNI. The characteristics of diffusive errors were consistent with those of dispersion errors. In full (spatial and temporal) discretization, matching SCNI for the stiffness matrix with GI for the mass matrix provided the best solution accuracy.

Acknowledgements

The support of this work by NSF/DARPA OPAAL Program under grant DMS 98-74015 and Sandia National Laboratories under the grant 5015 to the University of Iowa and UCLA is greatly acknowledged.

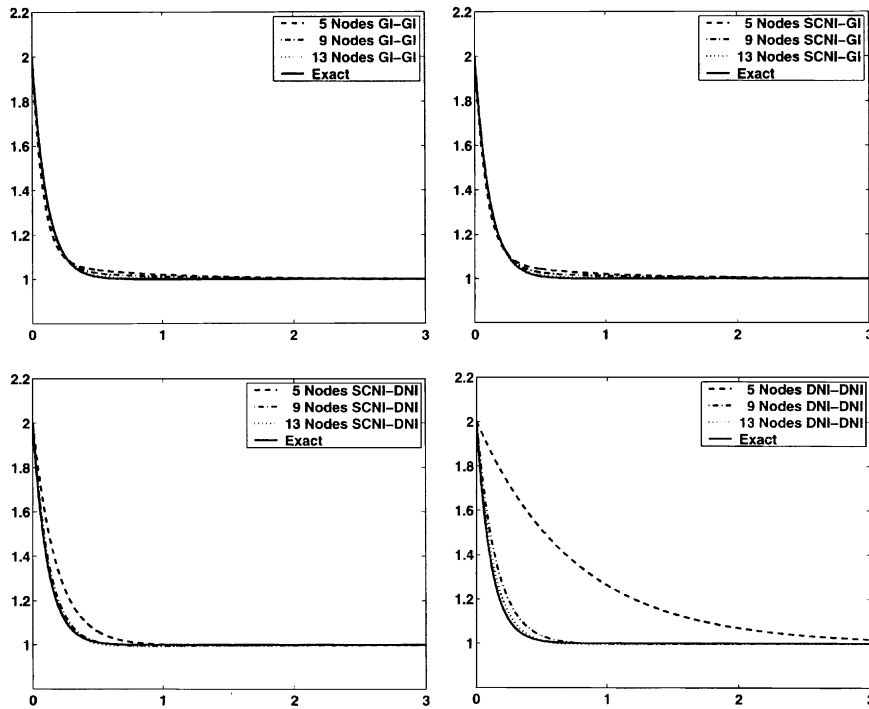


Fig. 14. Solution to heat equation with consistent capacity matrix.

References

- [1] T. Belytschko, Y.Y. Lu, L. Gu, Element-free Galerkin methods, *Int. J. Numer. Methods Eng.* 37 (1994) 229–256.
- [2] I. Babuska, J.M. Melenk, The partition of unity method, *Int. J. Numer. Methods Eng.* 40 (1997) 727–758.
- [3] C.A.M. Duarte, J.T. Oden, A h–p adaptive method using clouds, *Comput. Methods Appl. Mech. Eng.* 139 (1996) 237–262.
- [4] W.K. Liu, S. Jun, Y.F. Zhang, Reproducing kernel particle methods, *Int. J. Numer. Methods Fluids* 20 (1985) 1081–1106.
- [5] J.S. Chen, C. Pan, C.T. Wu, W.K. Liu, Reproducing kernel particle methods for large deformation analysis of nonlinear structures, *Comput. Methods Appl. Mech. Eng.* 139 (1996) 195–227.
- [6] J. Dolbow, T. Belytschko, Numerical integration of Galerkin weak form in meshfree methods, *Comput. Mech.* 23 (1999) 219–230.
- [7] J.S. Chen, C.T. Wu, S. Yoon, Y. You, Stabilized conforming nodal integration for Galerkin meshfree methods, *Int. J. Numer. Methods Eng.* 50 (2001) 435–466.
- [8] T. Voth, T.M. Christon, Discretization errors associated with reproducing kernel methods: one-dimensional domains, *Comp. Methods Appl. Mech. Eng.* 190 (2001) 2429–2446.
- [9] J.J. Monaghan, Why particle methods work, *SIAM J. Sci. Statist. Comput.* 3 (4) (1982) 422–433.